Photoacoustics 21 (2021) 100228

Contents lists available at ScienceDirect

Photoacoustics

journal homepage: www.elsevier.com/locate/pacs

Highly sensitive broadband differential infrared photoacoustic spectroscopy with wavelet denoising algorithm for trace gas detection

Lixian Liu [a,b,c,1], Huiting Huan [a,b,c,1], Wei Li [a], Andreas Mandelis [b,c], Yafei Wang [c], Le Zhang [a], Xueshi Zhang [a], Xukun Yin [a], Yuxiang Wu [a], Xiaopeng Shao [a,*]

[a] School of Physics and Optoelectronic Engineering, Xidian University, Xi'an, 710071, China
[b] Center for Advanced Diffusion-Wave and Photoacoustic Technologies (CADIPT), Department of Mechanical and Industrial Engineering, University of Toronto, Toronto, M5S 3G8, Canada
[c] School of Optoelectronic Information, University of Electronic Science and Technology of China, Chengdu, 610054, China

ARTICLE INFO

Keywords:
Noise elimination
Gas detection sensitivity
Fourier-transform infrared photoacoustic spectroscopy
Differential detection mode
Wavelet domain denoising

ABSTRACT

Enhancement of trace gas detectability using photoacoustic spectroscopy requires the effective suppression of strong background noise for practical applications. An upgraded infrared broadband trace gas detection configuration was investigated based on a Fourier transform infrared (FTIR) spectrometer equipped with specially designed T-resonators and simultaneous differential optical and photoacoustic measurement capabilities. By using acetylene and local air as appropriate samples, the detectivity of the differential photoacoustic mode was demonstrated to be far better than the pure optical approach both theoretically and experimentally, due to the effectiveness of light-correlated coherent noise suppression of non-intrinsic optical baseline signals. The wavelet domain denoising algorithm with the optimized parameters was introduced in detail to greatly improve the signal-to-noise ratio by denoising the incoherent ambient interference with respect to the differential photoacoustic measurement. The results showed enhancement of sensitivity to acetylene from 5 ppmv (original differential mode) to 806 ppbv, a fivefold improvement. With the suppression of background noise accomplished by the optimized wavelet domain denoising algorithm, the broadband differential photoacoustic trace gas detection was shown to be an effective approach for trace gas detection.

1. Introduction

Acetylene (C_2H_2) gas is widely used as a chemical building block and fuel for welding and cutting due to the high temperature of the flame. However, if initiated by intense heat or shock waves, C_2H_2 gas may decompose explosively due to its intrinsic instability especially when pressurized [1]. Hence, it is a safety priority to monitor acetylene leakage during industrial applications, storage and transport [2]. Conventional detectors for such flammable trace gas monitoring are usually based on chemical surface reactions, such as catalytic combustion which may require large amounts of energy for heating and may become toxic after a relatively short period [3].

Several spectroscopic methods [4–7] have been reported for trace C_2H_2 detection, and the sensitivity approaches ppb level with incident intensity of hundreds of milliwatts. In an environment of C_2H_2 leakage or explosion, the noise level caused by ambient turbulence, strongly absorbing background gases, and other interferences generated by the gas sensors themselves, is attributed to gas detection performance deterioration. Given equivalent optical energy density, eliminating strong interference during the measurement can essentially improve the gas sensors' performance. In order to suppress such noise and improve detection signal-to-noise ratio (SNR), various spectrometric designs have been proposed [8–14]. For example, laser calorimetry spectroscopy for dissolved C_2H_2 detection was introduced for removal of room temperature interference [15]. A dual-channel differential C_2H_2 detection system based on tunable diode laser absorption spectroscopy was established for the suppression of incident source turbulence [16]. Several signal processing algorithms were proposed for the improvement of gas detection sensitivity [17–19]. However, discussion on the noise constituents and the optimal choice of its suppression method are still absent and worthy of comprehensive modelling.

This work is devoted to analyzing the performance of coherent and

* Corresponding author at: School of Physics and Optoelectronic Engineering, Xidian University, Xi'an, 710071, China.
E-mail address: xpshao@xidian.edu.cn (X. Shao).
[1] H.H. and L.L. made equal contribution with respect to this work.

https://doi.org/10.1016/j.pacs.2020.100228
Received 5 October 2020; Received in revised form 28 November 2020; Accepted 3 December 2020
Available online 5 December 2020

incoherent noise suppression in an FTIR spectroscopic system based on optimal designing in configuration and signal processing algorithm: A simultaneous differential optical and photoacoustic mode detection method was proposed for suppressing the adverse effect of strongly overlapped background gases and other incident-light-related noise; The wavelet domain denosing (WDD) algorithm was introduced for removal of interferences generated by the ambient turbulence and the intrinsic noise of the sensors; The performance of the software-based denoising algorithms in terms of SNR and signal fidelity performance was systematically analyzed with a novel dual-evaluation criterion which helps seek the best combination of parameters in WDD configuration for removal of interferences generated by the ambient turbulence and the intrinsic noise of the sensors. The improved system with optimized WDD data processing exhibited over 5 times better detection sensitivity for acetylene given the same optical power.

2. Spectroscopic gas detection and noise evaluation setup

2.1. Experimental configuration

The use of broadband spectroscopic method for trace gas detection has the advantage of testing multiple target at the same time. However, it is also very dependent on the environmental noise level because of its low power incoherent source. This research was conducted with respect to an FTIR spectrometer to show the performance of noise suppression.

The trace gas detection experimental setup based on a Bruker Vertex 70 FTIR spectrometer is shown in Fig. 1. The incident light was modulated by a home-made mirror chopper with 50 % duty cycle, thereby avoiding beam splitting and ensuring maximum source intensity utilization [20]. The system was equipped with two identical sensitive T-type photoacoustic resonators and two mercury-cadmium-telluride (MCT, VIGO system® PV-2TE-8) detectors, assembled for the simultaneous acquisition of the differential photoacoustic and optical signals after interaction with the trace gas. Referring to a noisy testing situation, the sample resonator was filled with a mixture of target and absorbing background gases, while the reference resonator contained only the background gases. In order to balance the optical intensity incident in the two resonators, an iris was installed in the transmission beam path. The PA signals generated in the two T-resonators and the transmitted optical power intercepted by the two MCTs were ideally modulated out-of-phase respectively. Therefore, two signal mixers (Mini Circuits, ZFRSC-2050+) and lock-in amplifiers (LIA) were used for optical and photoacoustic signal mixing and demodulation, respectively. Single-ended mode optical power transmitted by the reference resonator was collected for use with trace gas absorption spectral normalization. This trace gas detection configuration allowed switching between the single-ended and differential modes of both the optical and photoacoustic signals only by changing mixer connections.

Since several absorption peaks of C_2H_2 lie within the water vapor absorption band, it was decided to use C_2H_2 and ambient lab air as chosen target and background gas, respectively, to test for elimination of the strongly overlapped background by means of the differential detection mode. The amplitude and phase responses of the two T-resonators are shown in Fig. 2. Their resonant frequency was around 342 Hz which was also used in differential test mode. The very similar frequency responses of the two resonators were a major criterion of good performance of the differential PA mode. More detailed description of the T-resonators was presented elsewhere [21].

The step-scan mode of the FTIR spectrometer was used for simultaneous acquisition of the differential PA and optical signals. The spectral range and resolution were set at 1000−9500 cm^{-1} and 6 cm^{-1}, respectively. The time constant of the lock-in amplifiers was set at 100 ms.

2.2. Wavelet domain denoising algorithm

Wavelet transforms, the projection of the signal onto the wavelet bases, have been successfully used in pattern recognition, image denoising, signal processing, and image compression [22–24]. In the wavelet domain, the signal has concentrated “energy’’ residing in just a

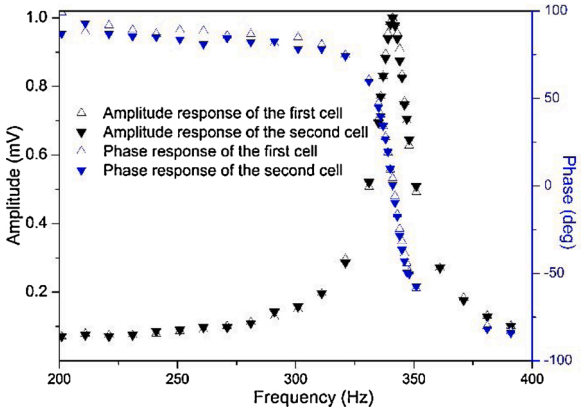

Fig. 2. Experimental results of the two PA T-cells.

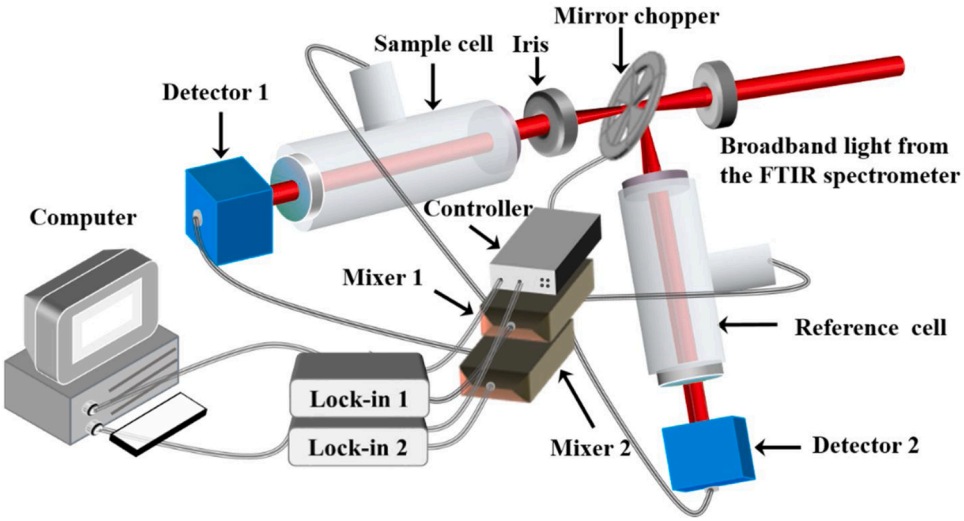

Fig. 1. Schematic of the experimental setup.

few high magnitude coefficients while the noise is represented by coefficients with small magnitudes. The sparsity of wavelet coefficients representing the signal is exploited by wavelet shrinkage methods to separate noise from signal coefficients. Unlike Fourier-based low-pass filter smoothing that eliminates high-frequency components, wavelet domain denoising removes a considerable amount of noise while preserving sharp (high-frequency) features in the signal. This is so because wavelets localize features in the observed data on different scales, so that one can shrink the wavelet domain by typically discarding the small value coefficients. Using orthogonal bases in different scales, the wavelet method has the advantage of multi-resolution that guarantees its effectiveness for noise elimination and SNR enhancement [25,26].

The principle of the differential configuration of spectroscopic system can facilitate less noisy spectra, but presumably incoherent noise still affects the spectral quality. The wavelet domain denoising (WDD) algorithms were adopted to eliminate the remaining signal and further improve spectra. The quality of trace gas absorption spectra processed by wavelet domain denoising (WDD) algorithms is mainly decided by the optimal wavelet function (wavelet mother basis), wavelet decomposition level (DL) and thresholds. Selection of a suitable wavelet function helps maximize coefficient values in the wavelet domain. Usually an appropriate wavelet function is determined by the specific practice requirements. There were 10 wavelet functions tested for the trace gas absorption spectral improvement, named “sym8”, “sym4”, “haar”, “db02”, “db08”, “coif1”, “coif3”, “bior2.2”, “fk4”, “fk8” [27]. Theoretically, WDD algorithms with higher wavelet DL produce better smoothness and noise removal results. Unfortunately, if processed with too high a value of wavelet DL, the absorption spectra may exhibit distortion and effective absorption information of trace gases may get lost. Matlab generated 1∼8 wavelet DLs in order to investigate the optimized behavior of denoising and absorption feature fidelity. Furthermore, four thresholds for shrinking wavelet coefficients and further improving denoising performance, named “rigrsure”, “heusure”, “sqtwologo” and “minimaxi” [28–30], are discussed in the Results and Discussion section of this paper.

3. Differential optical and photoacoustic mode trace gas detection principle

3.1. The differential optical and photoacoustic mode

As described in Sect. 2.1, the sample resonator was filled with the mixture of target and background gases. The reference resonator contained the background gas only. The incident optical signals of the two resonators are modulated by the mirror chopper. Consideration of the noise generated by the background gases alone yields the harmonic optical signals detected by the MCTs at wavenumber σ:

$$\begin{cases} I_t(\sigma) = I_0(\sigma)e^{-\left[\sum_k^T \alpha_k(\sigma)+\sum_{k'}^{T'}\alpha_{k'}(\sigma)\right]L}R_{MCT}(\sigma) \quad (1\text{-a}) \\ I_r(\sigma) = I_0(\sigma)e^{-\left(\sum_{k'}^{T'}\alpha_{k'}(\sigma)\right)L}R_{MCT}(\sigma)e^{i\varphi} \quad (1\text{-b}) \end{cases}$$

where I_t stands for the transmitted optical signal; I_r is the reflected optical signal. I_0 is the incident intensity of the two resonators. α_k represents the absorption coefficient of gaseous component (k) at each excitation wavelength. T is the total number of target gases, and T' is the total number of strongly absorbing residual (background) gases. L is the optical absorption length in the gas; $R_{MCT}(\sigma)$ is the optical response of the MCT detectors. φ is the phase difference of the two optical signals due to the mirror chopper modulation.

The gas absorption coefficients satisfy the optically thin condition $\alpha_k(\sigma)L \ll 1$, if only trace gas concentrations are measured in the detection system. The absorption coefficient of a desired gas (k) is defined as [19] $\alpha_k(\sigma) = N_{tot}c(k)E_k(\sigma)$; N_{tot} is the total number density of molecules; $c(k)$ and $E_k(\sigma)$ are the concentration and the absorption spectrum of the k-th component, respectively. The optical signals can be described as Eq. (2) according to the Taylor series expansion of Eq. (1).

$$\begin{cases} I_t(\sigma) = I_0(\sigma)R_{MCT}(\sigma)\left\{1 - \left[\sum_k^T c(k)E_k(\sigma) + \sum_{k'}^{T'} c(k')E_{k'}(\sigma)\right]N_{tot}L\right\} \quad (2\text{-a}) \\ I_r(\sigma) = I_0(\sigma)R_{MCT}(\sigma)\left\{1 - \left[\sum_{k'}^{T'} c(k')E_{k'}(\sigma)\right]N_{tot}L\right\}e^{i\varphi} \quad (2\text{-b}) \end{cases}$$

It is seen that, based on Eqs. (2), the differential optical signal is the sum of the two single mode data generated by multiple target gases and demodulated by LIA # 2 in Fig. 1 is given by:

$$\begin{aligned} I_d(\sigma) &= I_t(\sigma) + I_r(\sigma) \\ &= I_0(\sigma)R_{MCT}(\sigma)\left\{\left(1+e^{i\varphi}\right)\left[1 - \left(\sum_{k'}^{T'} c(k')E_{k'}(\sigma)\right)N_{tot}L\right] \right. \\ &\quad \left. - \left(\sum_k^T c(k)E_k(\sigma)\right)N_{tot}L\right\} \end{aligned} \quad (3)$$

which is independent of background gas contributions and the optical baseline (the factor “1” inside the first square bracket), if the incident light in the two resonators is modulated precisely out-of-phase. In that case, the differential optical signal $I_d(\sigma)$ is proportional to the sum of concentrations of the target gases.

It is clear that the optical baseline constitutes a more stubborn obstacle for target gas effective information extraction than the noise caused by the background gases due to their weak overlapping absorptions at wavenumber σ, $\left(\sum_{k'}^{T'} c(k')E_{k'}(\sigma)\right)N_{tot}L \ll 1$. Moreover, if φ slight deviates from π, the useful absorption features of an overlapped target gas are nearly impossible to measure optically because transmitted or reflected optical power change generated by the trace gas represents a relatively small reduction in the received optical power. This is a well-known fact that has led to the development of sophisticated optical spectrometers with multi-pass mirror designs to enhance the absorbed fraction of the incident radiation [31,32].

The single mode photoacoustic signals generated in the two resonators are shown in Eq. (4). S_t and S_r refer to the photoacoustic signals in the transmission and reflection paths. ω_0 is the resonance frequency; R_{mic} and C are the microphone response and cell constant of photoacoustic resonators, respectively.

$$\begin{cases} S_t(\sigma) = I_0(\sigma)CR_{mic}(\omega_0)\left[\sum_{k=1}^{T} c(k)E_k(\sigma) + \sum_{k'=1}^{T'} c(k')E_{k'}(\sigma)\right]N_{tot}L \quad (4\text{-a}) \\ S_r(\sigma) = I_0(\sigma)CR_{mic}(\omega_0)N_{tot}L\sum_{k'=1}^{T'} c(k')E_{k'}(\sigma) \quad (4\text{-b}) \end{cases}$$

Combining the single mode PA absorption data of the two resonators, the differential photoacoustic signal $S_d(\sigma)$ collected by LIA # 1, Fig. 1, can be described by Eq. (5),

$$\begin{aligned} S_d(\sigma) &= S_t(\sigma) + S_r(\sigma) \\ &= I_0(\sigma)R_{mic}(\omega_0)C\left[\left(1+e^{i\varphi}\right)\left(\sum_{k'}^{T'} c(k')E_{k'}(\sigma)\right) \right. \\ &\quad \left. + \left(\sum_k^T c(k)E_k(\sigma)\right)\right]N_{tot}L \end{aligned} \quad (5)$$

provided that only the noise produced by the background gases is taken into account [23].

By comparing Eqs. (3) and (4), it is obvious that the differential PA mode trace gas detection mode is more powerful and convenient than the optical mode for trace target gas observation, in view of the non-intrinsic optical baseline disturbance for the photoacoustic signal.

3.2. Noise elimination analysis

Sensitivity - the minimum detectable concentration $c_{\min}$ of a desired gas - is restricted by the noise level of the detection system. The system noise can be divided into coherent and incoherent components. The coherent noise is the spurious signal correlated to the incident light; the incoherent component refers to random background noise. If only one target gas component is considered in the sample resonator for simplification, the gas detection sensitivity $c_{s\text{-min}}$ of the single-ended PA signal can be expressed as

$$I_0(\sigma)R_{mic}(\omega_0)c_{s-\min}(k)E_k(\sigma)N_{tot}L = N_{b-g} + N_{window} + N_{wall} + N_I + N_T + N_E \tag{6}$$

where

$$N_{b-g} = I_0(\sigma)R_{mic}(\omega_0)C\sum_{k'}^{T} c(k')E_{k'}(\sigma)N_{tot}L \tag{7}$$

is the coherent noise caused by the background gases. N_{window} is the window heating coherent noise; N_{wall} is the coherent component generated by absorption and scattering of radiation on the resonator wall; and N_I is the coherent noise associated with incident light fluctuations. N_T and N_E represent thermal fluctuation and electrical noise, and they constitute the background incoherent noise.

The coherent noise generated in the two resonators is modulated by the mirror chopper in the differential mode PA system. Thus, the detection sensitivity $c_{d\text{-min}}$ of the differential mode photoacoustic system is given by

$$I_0(\sigma)R_{mic}(\omega_0)c_{d-\min}(k)E_k(\sigma)N_{tot}L = \left(N_{b-g} + N_{window} + N_{wall} + N_I\right)\left(1 + e^{i\varphi}\right) + N_T^{'} + N_E^{'} \tag{8}$$

where, $N_T^{'}$ and $N_E^{'}$ are the incoherent thermal and electrical noise, respectively. The coherent noise components N_{window}, N_{wall}, and N_I present in Eq. (6) are cancelled out by the differential mode's out-of-phase modulation as was also experimentally verified [19].

When the trace gas concentration is extremely low, the main interference in the differential PA mode is dominated by the incoherent noise which essentially remains at the same level throughout the entire spectral range and cannot be removed by experimental procedures. It is in this limiting case where the WDD algorithm developed in this work was applied for further noise suppression and SNR improvement. Denoising processing yields the differential mode PA sensitivity shown in Eq. (9),

$$I_0(\sigma)R_{mic}(\omega_0)c_{d'-\min}(k)E_k(\sigma)N_{tot}L = \mathrm{WDD}[N] \tag{9}$$

where N is the noise level of the differential mode PA system.

4. Results and discussion

4.1. The differential optical and photoacoustic performance

To validate the performance of spectroscopic differentiation that should be able to elliminate the identical components in the absorption spectra, two gas species were tested. The first experiment used nitrogen as a non-absorber and filled the two cell with identical gas to validate suppressing of systematic background noise, generated by factors irrelavent to gas absorption. As shown in Fig. 3, the conventional single mode optical spectrum clearly reflects the spectrum of the broadband source, while both optical and photoaoucstic differential spectra have nearly zero amplitude, which is in ideal accordance with the non-absorbing nature of nitrogen in the wavenumber range. The result implies that the differentiation can cancel the identical feature with respect to the sample and reference cells.

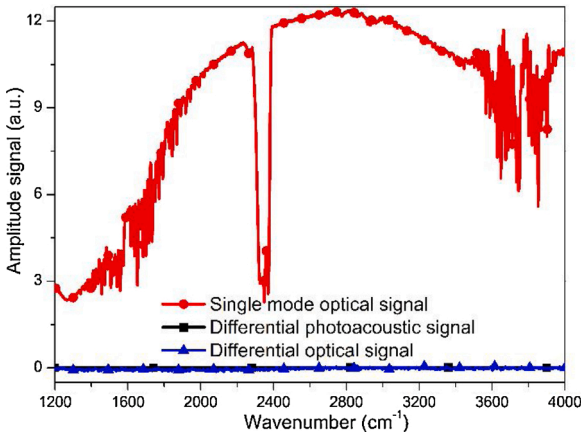

Fig. 3. Performance of differential optical and photoacoustic spectra in non-absorbing gas.

The second validation used acetylene (25 ppmv) and ambient air mixture as the preferred compound and the same ambient air as reference for differentiation. Considering the fact that a couple of absorption peaks (1302 and 1360 cm^{-1}) of acetylene lie within the water absorption band (1260−2000 cm^{-1}), the experiment can validate the ability of elliminating background gas absorption and revealing absorption information of target gas. Fig. 4 gives the collected trace gas spectra by three modes. All spectra were normalized by the optical source spectrum in the FTIR spectrometer.

The blue curve stands for the single-ended PA mode trace gas detection result, which is observed after dividing the signal of the sample resonator by that from the reference resonator. There are no distinguishable absorption features at the acetylene absorption peaks for the single PA mode due to significant inteference from background gases. Similarly, the presence of the inherent optical baseline prevents the appearance of absorption peaks even in the differential optical mode—the dashed curve close to zero in Fig. 4. It is concluded that the optical gas detection method with such a short absorption path (~80 mm) has no ability to yield trace gas absorption information at concentrations below 25 ppmv. Only the differential PA mode reveals the acetylene absorption peaks, a fact that further demonstrates its ability to suppress coherent noise and eliminate background gas interfering absorption.

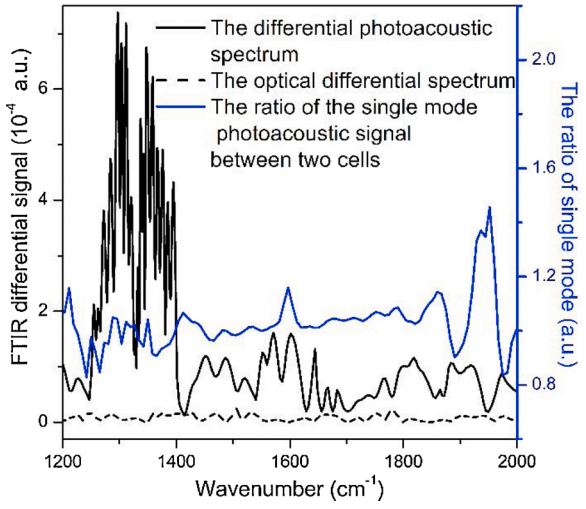

Fig. 4. Three modes spectra of 25 ppmv acetylene and ambient air.

4.2. Trace gas absorption spectra processed by the wavelet domain denoising algorithm

It is noted that incoherent noise interference remains and dominates the noise floor in the differential PA spectrum in Fig. 4. Therefore, the WDD algorithms were used to suppress that noise. The SNR performance of the denoising for the differential PA spectra of 25 ppmv acetylene is shown in the histograms of Fig. 5. The SNR of the differential mode PA spectra was calculated as the ratio of the acetylene absorption peak (1360 cm^{-1}) value to the system noise level. To calculate the noise level, a straight line was fitted to the spectrum in the region where no gas absorption occurs (2800–3050 cm^{-1}). The deviation between the best-fit straight line and the experimental data was used as the noise floor of the denoised results.

There are 10 wavelet functions and 8 wavelet DLs presented in each histogram of Fig. 5. The thresholds are selected as “rigrsure”, “heusure”, “sqtwologo” and “minimaxi”, respectively. The results with the 1st DL represent the original spectral SNR which is significantly improved by the WDD method. It is seen from the SNR structure of Fig. 5 that the incoherent noise level is dramatically suppressed by means of the WDD algorithm. Nevertheless, there were spectral distortions in the acetylene absorption features after the WDD algorithm was applied. The SNR is always discussed as the sole criterion for the evaluation of the spectral denoising performance in the published literature [30,31]. Therefore, the criteria for the performance of spectrum processing in this paper should include two aspects, i.e. the SNR improvement and limited spectrum distortion. In order to evaluate the absorption peak distortion between original and processed spectra, the structural similarity (SSIM) was evoked for evaluation of effective information fidelity.

$$SSIM(s_d, s_{d'}) = \frac{(2\mu_d\mu_{d'} + c_1)(2\sigma_{d,d'} + c_2)}{(\mu_d^2 + \mu_{d'}^2 + c_1)(\sigma_d^2 + \sigma_{d'}^2 + c_2)} \tag{10}$$

where s_d is the original signal; $s_{d'}$ is the processed signal; μ_d is the average of s_d; $\mu_{d'}$ is the average of $s_{d'}$; σ_d^2 is the variance of s_d; $\sigma_{d'}^2$ is the variance of $s_{d'}$; $\sigma_{d,d'}$ is the covariance of s_d and $s_{d'}$; $c_1=(k_1D)^2$, $c_2=(k_2D)^2$ are two variables used to stabilize the division with weak (~ near zero) denominators; D is the signal dynamic range; $k_1 = 0.01$ and $k_2 = 0.03$ are constants by default [32].

To analyze the spectrum fidelity performance of the WDD algorithms, 17 processing methods with the SNR larger than 120 in Fig. 5 were selected to carry out similarity analysis of the original and processed absorption features. The original spectrum was processed with these selected methods and SSIM indices were calculated with respect to the absorption region (1275 cm^{-1} - 1400 cm^{-1}). The WDD algorithms involve three important parameters, the combinations of which result in different level of SSIM and SNR values shown in Fig. 6. The four different regions represent the four thresholds used during the denoising process. The different colors and filling patterns of each bar refer to the DLs and wavelet functions, respectively. The numbers on top of the bars are the corresponding SNR processed by the denoising methods shown in Fig. 5. It is obvious that the results processed with the threshold “rigrsure” present an optimal fidelity of the spectral peaks due to the fact that SSIM is greater than 0.95 for all the bars in the light pink region. There are 6 bars processed with “db08” in Fig. 6, which occupy the largest proportion among all the wavelet functions. Hence the threshold “rigrsure” and the wavelet function “db08” are the preferred parameters during the WDD processing algorithms for photoacoustic spectra. Although the larger the adopted DL, the smoother the spectra become, it causes the

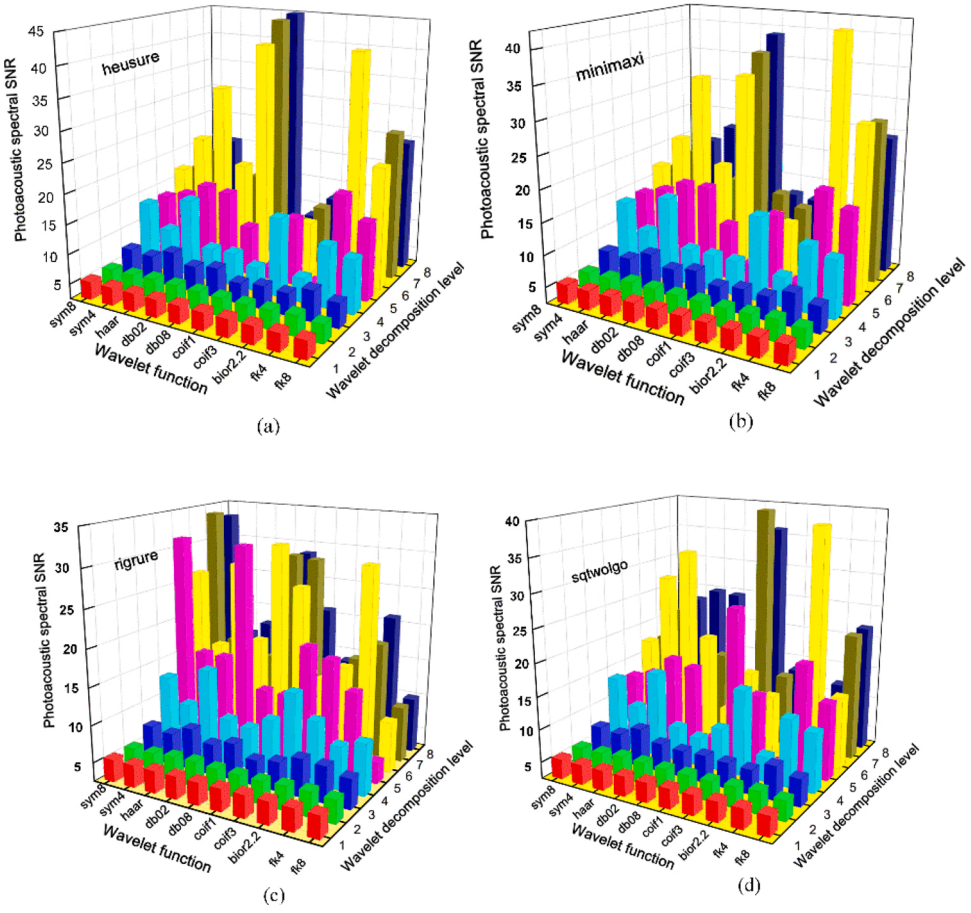

Fig. 5. The PA spectral SNR improvement by means of WDD denoising methods.

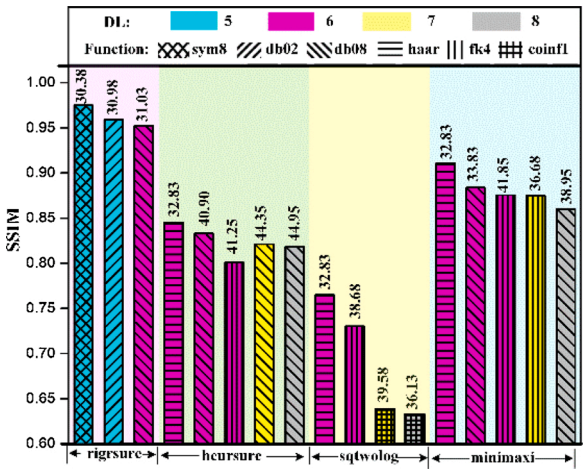

Fig. 6. The spectral SSIM processed by denoising methods.

distortion of valuable absorption peaks, which explains why the spectra denoised by 6th DL (the rosy red bars) exhibit the maximal SNR, greater than 120. Therefore, the DL selection needs to balance noise level suppression (SNR) and effective information loss (SSIM).

To clarify the performance of the denoised results, we chose three groups of WDD processing methods and the results are shown in Fig. 7. The processed spectrum with wavelet function-"sym8", DL-5 and threshold-"rigrsure" introduces conspicuous but spurious peaks around 2300 cm^{-1} nevertheless it exhibits the maximal SSIM. Compared with the original differential PA spectrum of 25 ppmv acetylene depicted in Fig. 7(a), the absorption spectrum at 3294 cm^{-1} of the maximum SNR spectrum (Fig.7(d), the results with the maximal SNR possessed by the combination wavelet function-"db08", DL-8 and threshold-"heursure") presents an obvious distortion with unexpected small peaks, which coincides with its low corresponding SSIM (~0.83). Considering both system improvement and peak feature fidelity characteristics, the WDD algorithm with the optimal parameters as wavelet function "db08", DL 6, and threshold "rigrsure" (shown in Fig. 7(c)) was used for the gas detection sensitivity, dynamic range and detection prescision analysis of the differential photoacoustic system in the next sections.

4.3. Limit of detection and amplitude-concentration dependence

As implied by Fig. 5, the SNR for the 25 ppmv acetylene original spectrum is 5.42, thus the limit of detection (LOD) of the differential PA mode was 5 ppmv (25 ppmv/5.42). After applying the optimal WDD algorithm ("rigrsure", "db08", 6) the spectral SNR yields 31.03, and the calculated LOD of acetylene was also improved to 806 ppbv (25 ppmv/31.03). Scaling to equivalent incident light intensity, the DPAS with the optimized WDD algorithm revealed better performance and lower trace detection limit than several other laser absorption methodologies, as shown in Table 1. Thanks to the broadband emission feature of FTIR sources, the stronger absorption peaks are used as compensation for their lower emitting power compared with lasers. Therefore, by virtue of the differential photoacoustic mode and the optimized wavelet denoising method, sub-ppmv level trace gas detection sensitivity was achieved with only 30 μW optical intensity of the FTIR spectrometer source at 1360 cm^{-1}.

Several designated concentration gas samples within 0–5000 ppmv were measured and plotted in Fig. 8. The differential PA spectra of each acetylene concentration sample were the average of 10 measured data. Fig. 8 shows the acetylene absorption peak (1360 cm^{-1}) values vs. concentration. The experimental data processed by the WDD algorithm exhibit the expected linear dependence on acetylene concentration. Both the correlation coefficient (R^2) and root mean square error (RMSE) of the WDD augmented data are better than the fitting results of the original spectra.

4.4. Improvement in gas detection precision and procedure

The precision of trace gas detection by this technique is described by the relative detection errors estimated by the standard deviation of the 10 measured data for each acetylene concentration. The relative detection errors with/without the WDD algorithm are shown in Fig. 9. The relative errors from measurements processed by the WDD algorithm less than half those of the original differential PA spectra. It is thus concluded that the proposed wavelet denoising method was proven to

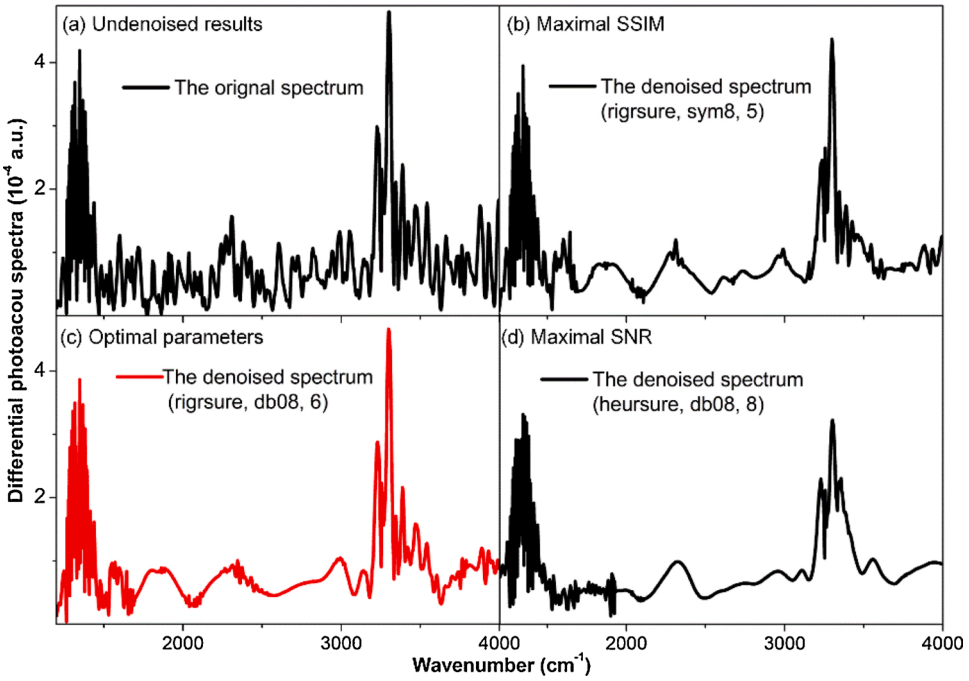

Fig. 7. The denoised differential PA spectra of 25 ppmv acetylene.

Table 1
Trace gas detection results comparisons.

Gas	Technique	Incident source/Power	Absorption peak (cm^{-1})	Absorption cross-section (cm^2/molecule)	Background gas	Denoising method	LOD
CH_4	FTIR-PAS	Bruker FTIR source	3017	1.49×10^{-18}	N_2	/	0.5 ppm [35]
H_2S	QEPAS[1]	QCL[3]/1.1 mW	97.11	5.75×10^{-21}	N_2	/	30 ppm [36]
CO_2	TDLAS[2]	DFB laser	4978.2	3.79×10^{-22}	N_2	Kalman filter	61.9 ppm [37]
CO	TDLAS	DFB[4] laser/ 20 mW	6380.32	1.02×10^{-22}	N_2	EMD[5]	2 ppm [38]
CO_2	FTIR-PAS	Bruker FTIR source /8 μW	2349	6.50×10^{-18}	Air	/	2ppmv [20]
C_2H_2	DPAS	Bruker FTIR source /30 μW	1360	2.78×10^{-19}	Air	WDD	806 ppbv [This paper]

[1] QEPAS: quartz enhanced photoacoustic spectroscopy.
[2] TDLAS: tunable diode laser absorption spectroscopy.
[3] QCL: quantum cascade laser.
[4] DFB laser: distributed feedback laser.
[5] EMD: empirical mode decomposition algorithm.

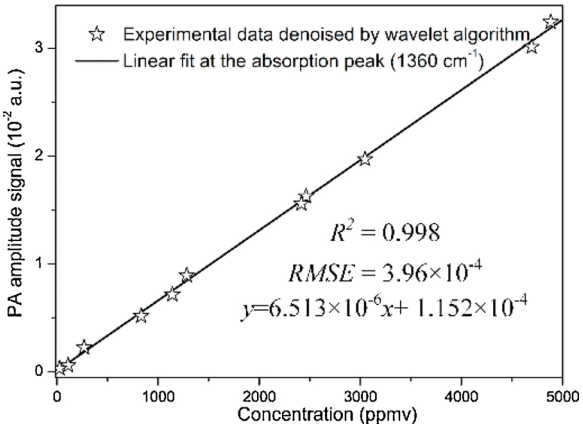

Fig. 8. Photoacoustic amplitude response vs. concentration.

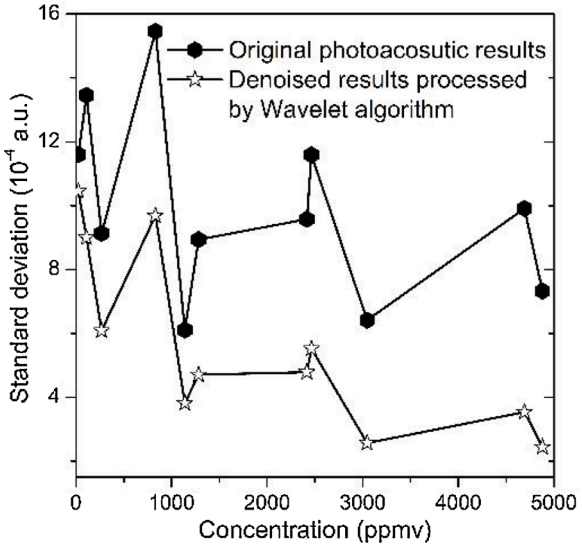

Fig. 9. Differential PA amplitude response vs. concentration.

be very effective for considerable gas detection precision improvements.

Finally, based on the foregoing analysis and results, the impoved trace gas detection procedure with broadband differential method is shown in the flowchart of Fig. 10. WDD processing was introduced after we obtained the original spectra from the spectrometer. Absorption peaks of the target gases and the noise levels of the collected spectra were improved. The optimized parameters ("rigrsure", "db08″, 6) of the

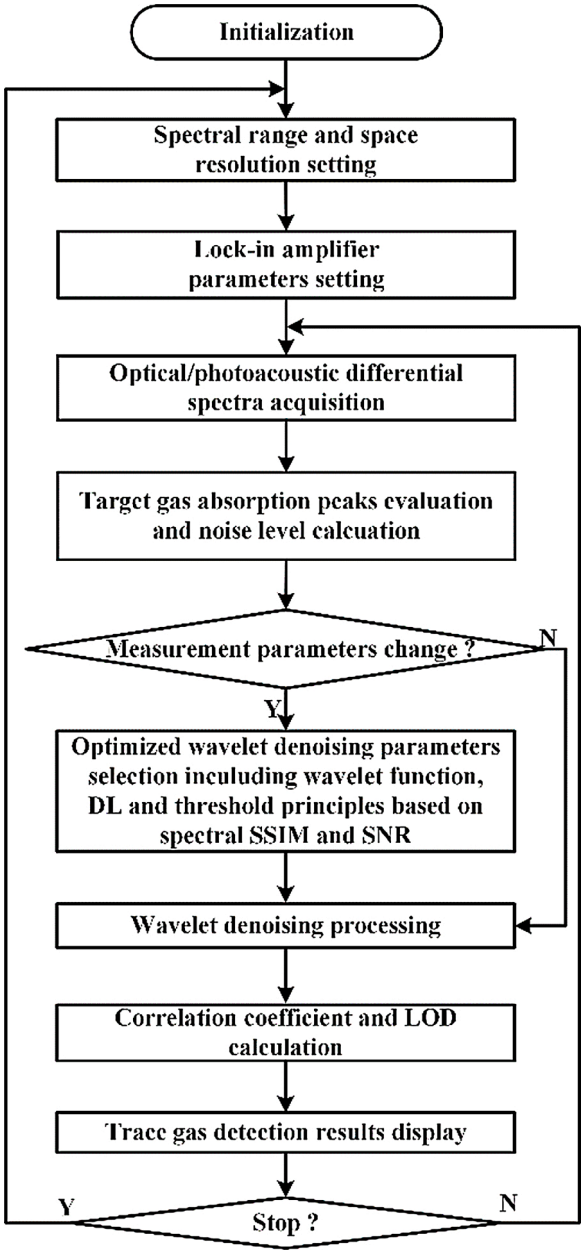

Fig. 10. The trace gas detection calculation flowchart with the differential mode and WDD algorithm.

WDD algorithm were recalculated in case of measurement parameter changes. The theoretical gas detection sensitivity was estimated to quantify the noise suppression performance of the differential modes and the WDD algorithms. The trace gas detection system returned to the initialization status after receiving the "stop" instruction. Otherwise, the system would continue collecting and processing absorption data.

5. Conclusions

A WDD algorithm-enhanced dual-differential broadband trace gas detection technique was presented and was shown to be capable of suppressing residual background noise, thereby substantially improving sensitivity over the original DFTIR-PAS method. The suppression of coherent and incoherent noise in a PA system was analyzed theoretically and experimentally with the use of differential modality and WDD algorithms. The optimized WDD algorithm was investigated in terms of the wavelet function "db08", DL 6, and threshold "rigrsure". The acetylene gas detection sensitivity was improved more than 5 times to 806 ppbv with 30 μW incident light power.

In conclusion, by virtue of the effective noise elimination afforded by the application of wavelet denoising, the broadband differential FTIR PAS trace gas detection system was demonstrated to be a sensitive and robust broadband spectroscopic approach for trace gas detection. Compared with laser spectroscopic method, the augmented FTIR PAS system achieves broadband spectroscopy with less energy but excellent detectability.

Declaration of Competing Interest

The authors declare that there are no conflicts of interest.

Acknowledgements

The authors are grateful to the National Science Foundation of China (Grant No. 61805187 and 61801358) and China Postdoctoral Science Foundation (Grant No. 2019M653546, 2019M653547). This work was also supported by "the Fundamental Research Funds for the Central Universities" (Grant No. JB20190412 and XJS190505). H.H. and L.L. acknowledge the Natural Science Foundation of Shaanxi Province with Grant No. 2019JQ-651 and 2020JQ-293. Special thanks are given to the Natural Sciences and Engineering Research Council of Canada (NSERC) for a Discovery Grant to A. Mandelis and the Chinese Recruitment Program of Global Experts (Thousand Talents).

References

[1] V.I. Babushok, A.W. Miziolke, Condensation flame of acetylene decomposition, Combust. Flame 136 (2004) 141–145.
[2] J.W.H. Price, An acetylene cylinder explosion: a most probable cause analysis, Eng. Fail. Anal. 13 (2006) 705–715.
[3] F. Bertocci, A. Fort, V. Vignoli, L. Shahin, M. Mugnaini, R. Berni, Assessment and optimization for novel gas materials through the evaluation of mixed response surface models, IEEE Trans. Instrument. Measur. 64 (10) (2015) 1084–1092.
[4] A.S.M. Iftekhar Uddin, U. Yaqoob, D. Phan, G. Chung, A novel flexible sensor based on PI/PTFE-supported Ag-loaded vertical ZnO nanorods array, Sens. Actuators B Chem. 222 (2016) 536–543.
[5] Y. Ma, Y. He, L. Zhang, X. Yu, J. Zhang, R. Sun, Ultra-high sensitive acetylene detection using quartz-enhanced photoacoustic spectroscopy with a fiber amplified diode laser and a 30.7 kHz quartz tuning fork, Appl. Phys. Lett. 110 (2017), 031107.
[6] F. Yang, Y. Tan, W. Jin, Y. Lin, Y. Qi, H. Ho, Hollow-core fiber Fabry-Perot photothermal gas sensor, Opt. Lett. 41 (2016) 3025–3028.
[7] A. Yolalmaz, F.H. Sadroud, M.F. Danisman, O. Esenturk, Intracavity gas detection with fiber loop ring down spectroscopy, Opt. Commun. 396 (2017) 141–145.
[8] Y. He, Y. Ma, Y. Tong, X. Yu, F.K. Tittel, Ultra-high sensitive light-induced thermoelastic spectroscopy sensor with a high Q- factor quartz tuning fork and a multipass cell, Opt. Lett. 44 (2019) 1904–1907.
[9] H. Wu, L. Dong, H. Zheng, Y. Yu, W. Ma, L. Zhang, W. Yin, L. Xiao, S. Jia, F. K. Tittel, Beat frequency quartz-enhanced photoacoustic spectroscopy for fast and calibration-free continuous trace-gas monitoring, Nat. Commun. 8 (2017) 15331.
[10] X. Liu, S. Cheng, H. Liu, S. Hu, D. Zhang, H. Ning, A survey on gas sensing technology, Sensors 12 (7) (2012) 9635–9665.
[11] P. Patimisco, A. Sampaolo, H. Zheng, L. Dong, F.K. Tittel, V. Spagnolo, Quartz-enhanced photoacoustic spectrophones exploiting custom tuning forks: a review, Adv. Phys.:X 2 (1) (2017) 169–187.
[12] X. Yin, H. Wu, L. Dong, B. Li, W. Ma, L. Zhang, L. Xiao, S. Jia, F.K. Tittel, Ppb-level SO_2 photoacoustic sensors with a suppressed absorption desorption effect by using a 7.41μm external cavity quantum cascade laser, ACS Sens. 5 (2) (2020) 549–556.
[13] H. Zheng, Y. Liu, H. Lin, R. Kan, L. Dong, W. Zhu, J. Fang, J. Yu, F.K. Tittel, Z. Chen, Quartz-enhanced photoacoustic spectroscopy exploiting a fast and wideband electro-mechanical light modulator, Opt. Express 28 (19) (2020) 27966–27973.
[14] P. Patimisco, G. Scamarcio, F.K. Tittel, V. Spagnolo, Quartz-enhanced photoacoustic spectroscopy: a review, Sensors 14 (4) (2014) 6165–6206.
[15] K.S. Nagapriya, S. Shashank, R. Prashan, P. Samhitha, C. Gunaranjan, B. Anandaroop, C. Niloy, M. Saroj, M. Sandip, Laser calorimetry spectroscopy for ppm-level dissolved gas detection and analysis, Sci. Rep. 7 (2017) 42917.
[16] Z. Gong, K. Chen, Y. Yang, X. Zhou, W. Peng, Q. Yu, High-sensitivity fiber-optic acoustic sensor for photoacoustic spectroscopy based trace gas detection, Sens. Actuators B Chem. 247 (2017) 290–295.
[17] J. Li, B. Yu, W. Zhao, W. Chen, A review of signal enhancement and noise reduction for tunable diode laser absorption spectroscopy, Appl. Spectrosc. Rev. 49 (2014) 666–691.
[18] K. Zheng, C. Zheng, Q. He, D. Yao, L. Hu, Y. Zhang, Y. Wang, F.K. Tittel, Near-infrared acetylene sensor system using off-axis integrated-cavity output spectroscopy and two measurement schemes, Opt. Express 20 (2018) 26205–26216.
[19] C.T. Zheng, W.L. Ye, G.L. Li, X. Yu, C.X. Zhao, Z.W. Song, Y.D. Wang, Performance enhancement of a mid-infrared CH_4 detection sensor by optimizing an asymmetric ellipsoid gas-cell and reducing voltage-fluctuation: theory, design and experiment, Sens. Actuators B Chem. 160 (2011) 389–398.
[20] L. Liu, A. Mandelis, H. Huan, A. Melnikov, Step-scan T cell based differential Fourier transform infrared photoacoustic spectroscopy (DFTIR-PAS) for detection of ambient air contaminants, Appl. Phys. B 122 (2016) 268.
[21] L. Liu, A. Mandelis, H. Huan, K.H. Michaelian, A. Melnikov, Step scan T cell Fourier-transform infrared photoacoustic spectroscopy (FTIR-PAS) for detection of ambient air contaminants, Vib. Spectrosc. 87 (2016) 94–98.
[22] Y.Y. Tang, L.H. Yang, J. Liu, Wavelet Theory and Its Application to Pattern Recognition, World Scientific, 2000.
[23] S.G. Chang, Y.U. Bin, Adaptive wavelet thresholding for image denoising and compression, IEEE Trans. Image Proc. Publ. IEEE Signal Proc. Soc. 9 (9) (2000) 1532.
[24] A.S. Lewis, G. Knowles, Image compression using the 2-D wavelet transform, IEEE Trans. Image Process. 1 (2) (2002) 244–250.
[25] Y. Kopsinis, S. McLaughlin, Development of EMD-based denoising methods inspired by wavelet thresholding, IEEE Trans. Signal Proc. 57 (4) (2009) 1351–1362.
[26] S.G. Chang, B. Yu, M. Vetterli, Adaptive wavelet thresholding for image denoising and compression, IEEE Trans. Image Process. 9 (9) (2000) 1532–1546.
[27] S. Mallat, A theory for multiresolution signal decomposition: the wavelet representation, IEEE Trans. Pattern Anal. Mach. Intell. 11 (7) (1989) 674–693.
[28] D.L. Donoho, Progress in Wavelet analysis and WVD: a ten minute tour, in: Y. Meyer, S. Roques (Eds.), Progress in Wavelet Analysis and Applications, Gif-sur-Yvette: Editions Frontières, 1993.
[29] D.L. Donoho, I.M. Johnstone, Ideal spatial adaptation by Wavelet shrinkage, Biometrika 81 (1994) 425–455.
[30] D.L. Donoho, De-noising by soft-thresholding, IEEE Trans. Inf. Theory 42 (3) (1995) 613–627.
[31] B. Tuzson, M. Mangold, H. Looser, A. Manninen, L. Emmenegger, Compact multipass optical cell for laser spectroscopy, Opt. Lett. 38 (3) (2013) 257–259.
[32] C. Robert, Simple, stable, and compact multiple-reflection optical cell for very long optical paths, Appl. Opt. 46 (22) (2007) 5408–5418.
[35] C.B. Hirschmann, J. Uotila, S. Ojala, J. Tenhunen, R.L. Keiski, Fourier transform infrared photoacoustic multicomponent gas spectroscopy with optical cantilever detection, Appl. Spectrosc. 64 (3) (2010) 293–297.
[36] V. Spagnolo, P. Patimisco, R. Pennetta, A. Sampaolo, G. Scamarcio, M.S. Vitiello, F. K. Tittel, THz quartz-enhanced photoacoustic sensor for H_2S trace gas detection, Opt. Express 23 (6) (2015) 7574–7582.
[37] M. Niu, P. Han, L. Song, D. Hao, J. Zhang, L. Ma, Comparison and application of wavelet transform and Kalman filtering for denoising in δ^{13} CO_2 measurement by tunable diode laser absorption spectroscopy at 2.008 μm, Opt. Express 25 (20) (2017) A896–A905.
[38] Y. Meng, T. Liu, K. Liu, J. Jiang, R. Wang, T. Wang, H. Hu, A modified empirical mode decomposition algorithm in TDLAS for gas detection, IEEE Photonics J. 6 (6) (2014) 1–10.

Lixian Liu received her B.S. degree of electronic science and technology and doctorate in optical engineering from the University of Electronic Science and Technology of China, in 2012 and 2017, respectively. She is now a full-time lecturer in the School of Physics and Optoelectronic Engineering, Xidian University. Her research field is photoacoustic and optical spectroscopy technologies.

Huiting Huan received his B.S. and Ph.D degrees from the University of Electronic Science and Technology of China in 2012 and 2017, respectively. He is now a researcher and lecturer with the School of Mechano-Electronic Engineering, Xidian University. His main research field includes acoustic, electromagnetic and thermal radiometric non-destructive testing.

Wei Li received his bachelor degree in 2016 from the College of Electronic Science and Technology, Xidian University. Now he is a PhD student in the Optical Engineering College. His research interests include wavefront sensing, computational imaging and signal processing.

Andreas Mandelis received his B.S. degree in physics from Yale University, New Haven, CT, USA in 1974, followed by M. A., M.S.E., and Ph.D degrees in applied physics and materials science from Princeton University, Princeton, NJ, USA in 1976, 1977 and 1979, respectively. He is a Full Professor of mechanical and industrial engineering; electrical and computer engineering; and the Institute of Biomaterials and Biomedical Engineering, University of Toronto, Toronto, ON, Canada. He is the Director of the Center for Advanced Diffusion-Wave and Photoacoustic Technologies (CADIPT), Toronto. He is an author and coauthor of more than 410 scientific papers in refereed journals and 190 scientific and technical proceedings papers. He is the Editor-in-Chief of the Springer Nature International Journal of Thermophysics, and an Editor of the Journal of Biomedical Optics and the Journal of Applied Physics.

Yafei Wang is a full time professor at the University of Electronic Science and Technology of China. His field is the laser and optoelectronic detection, and nondestructive testing based on photoacoustic and photothermal technology.

Le Zhang is a Ph.D. student at the School of Physics and Optoelectronic Engineering, Xidian University. His research interests include photoacoustic spectroscopy and its application to trace gas detection.

Xueshi Zhang is a graduate student at the School of Physics and Optoelectronic Engineering, Xidian University. He focuses on the high sensitivity trace gas detection technology.

Xukun Yin received his Ph.D. degree in atomic and molecular physics from Shanxi University, China, in 2020. From 2018–2019, he studied as a research associate in the electrical and computer engineering department, Rice University, Houston, USA. Currently he is an assistant professor in the School of Physics and Optoelectronic Engineering of Xidian University. His research interests include optical sensors and laser spectroscopy techniques.

Yuxiang Wu received his PhD degree at University of Electronic Science and Technology of China in 2017. He is now a lecturer at Xidian University. His research interests is optical 3D measurement.

fx**10Xiaopeng Shao** received his Ph.D degree from Xidian University in 2005. He is a professor at the School of Physics and Optoelectronic Engineering, Xidian University. His research focuses on computational imaging, optical sensing and signal processing.